Influence of injected charge carriers on photocurrents in polymer solar cells

Wehenkel, Dominique J.; Koster, L. Jan Anton; Wienk, Martijn M.; Janssen, Rene A. J.

Published in:
Physical Review B

DOI:
10.1103/PhysRevB.85.125203

Publication date:
2012

Influence of injected charge carriers on photocurrents in polymer solar cells

Dominique J. Wehenkel, L. Jan Anton Koster, Martijn M. Wienk, and René A. J. Janssen
Molecular Materials and Nanosystems, Eindhoven University of Technology, PO Box 513, 5600 MB Eindhoven, The Netherlands
(Received 26 December 2011; revised manuscript received 19 February 2012; published 22 March 2012)

We determine and analyze the photocurrent J_{ph} in polymer solar cells under conditions where, no, one, or two different charge carriers can be injected by choosing appropriate electrodes and compare the experimental results to simulations based on a drift-diffusion device model that accounts for photogeneration and Langevin recombination of electrons and holes. We demonstrate that accounting for the series resistance of the device is essential to determine J_{ph}. Without such correction, the results are, even qualitatively, incorrect. We show that in solar cells with forward bias applied J_{ph} is reduced by recombination of photogenerated charge carriers with injected charge carriers. Self-selective contacts or band bending are not necessary to explain the effects. Without injecting contacts J_{ph} is symmetric around the compensation voltage. A simple analytical model shows that under high forward bias J_{ph} scales inversely with $1 + \xi\gamma_{pre}$, in which γ_{pre} represents the extent of Langevin recombination and ξ is a positive constant. Under conditions where Langevin recombination is very low or when electron and hole mobility are a very different, photogenerated charge carriers can affect the space-charge field and modify the injection of charge carriers. We show by simulations and experimentally that under such conditions the photocurrent can exceed that charge generation such that, effectively, photocurrent multiplication occurs.

DOI: 10.1103/PhysRevB.85.125203 PACS number(s): 72.80.Le, 73.50.Pz, 72.20.Jv, 71.23.An

I. INTRODUCTION

Polymer solar cells generally consist of two complementary organic semiconductors with offset energy levels.[1] Absorption of light in either of the two materials produces an exciton which dissociates into electrons and holes when it diffuses to the interface of the two semiconductors. Because the exciton diffusion length in organic semiconductors is limited to about 10 nm, polymer solar cells often use a bulk heterojunction architecture in which the two materials are mixed into an interpenetrating nanoscopic network to ensure efficient exciton dissociation. Polymer solar cells further use two electrodes with different work functions to create a built-in electrical field that causes the photogenerated electrons and holes to be separated spatially and be collected. Hence, the work function difference of the two electrodes determines the polarity of the device and limits its open circuit voltage V_{oc}, provided the difference is less than the energy of the interfacial charge-separated state.[2,3] To maximize V_{oc}, the electrode materials are chosen such that their work functions are able to create Ohmic contacts with the photoactive layer.[4] This is achieved when the work function of the hole-collecting contact aligns with the highest occupied molecular orbital (HOMO) level of the electron donor, *p*-type material, and that of the electron-collecting contact aligns with the lowest unoccupied molecular orbital (LUMO) of the electron acceptor, *n*-type material.

In this particular alignment of energy levels the device acts as a diode in the dark because carriers can be injected and transported through the device only for voltages higher than the built-in voltage (forward bias). Under illumination and in reverse bias, where injection is largely inhibited, the current is determined by the amount of photogenerated free charge carriers, their transport through the active layer, the recombination between carriers, and their collection at the electrode. In forward bias, the situation is more complex because injected and photogenerated carriers are present simultaneously. In optimizing the performance of polymer solar cells the electric field dependence of the photocurrent density J_{ph}, defined as the difference between the illumination (J_{light}) and dark (J_{dark}) current densities, $J_{ph} = J_{light} - J_{dark}$, is an important parameter. Ideally, J_{ph} would be weakly dependent on the electric field because this would maximize the fill factor (FF) of the solar cell and thereby the power conversion efficiency.

One way to probe the electric-field dependence of photogenerated carriers is to measure the photocurrent. In reverse bias, where the dark current is virtually zero, the photocurrent is equal to the illumination current ($J_{ph} = J_{light}$). However, in forward bias, where also the injected charges contribute, the photocurrent cannot be determined reliably from standard current density–voltage (J-V) measurements. Ooi *et al.* demonstrated that the photocurrent is easily overestimated under illumination since the sample heats up such that the dark and illumination currents are measured at different temperatures.[5] An elegant solution to suppress the effect of heating the substrate under illumination is to use a pulsed white light-emitting diode (LED).[5] By keeping the on-off cycles of the LED shorter than the cooling and heating time of the sample, the dark and illumination currents are measured at the same temperature.

With this technique Ooi *et al.* studied photocurrent generation in poly(3-hexylthiophene):[6,6]phenyl-C_{61}-butyric acid methyl ester (P3HT:PCBM) solar cells sandwiched between a transparent indium tin oxide electrode covered with poly(3,4-ethylenedioxythiophene):polystyrenesulfonate (PEDOT:PSS) and an aluminum back electrode. They observed that the J_{ph}-V curve is nearly symmetric around a well-defined point called the point of optimal symmetry (POS).[5] The POS is observed to occur at a nonzero photocurrent such that the photocurrent is asymmetric around $J_{ph} = 0$ and hence different under forward bias as compared to reverse bias. According to Ooi *et al.*, the POS is located at the built-in voltage ($V_{pos} = V_{bi}$) and corresponds to the flat-band condition of

the solar cell. The J_{ph}-V curve can be decomposed into a voltage (field) dependent $J_{ph}(V)$ component and a constant voltage-independent $J_{ph}(V_{pos})$ component. Ooi *et al*. explained that the voltage-independent $J_{ph}(V_{pos})$ component results from a net diffusive photocurrent due to self-selective electrodes. A self-selective electrode is an electrode which collects only one type of charge carrier and blocks the other type of carrier. The field-dependent photocurrent $J_{ph}(V)$, which results from an improved extraction of carriers with increasing electric field, is shifted by the constant diffusive photocurrent $J_{ph}(V_{pos})$.

Limpinsel *et al*. also studied the photocurrent in P3HT:PCBM solar cells and made very similar observations but presented an alternative explanation.[6] Limpinsel *et al*. agree that the J_{ph}-V curve consists of a voltage-independent $J_{ph}(V_{pos})$ and a voltage-dependent $J_{ph}(V)$ component. However, Limpinsel *et al*. do not agree on the origin of the POS and of the voltage-independent photocurrent component of the J_{ph}-V curves. They consider that at the POS (V_{pos}) the solar cell is not at flat-band condition but rather at a quasi-flat-band condition, well below V_{bi}.[6] At the POS the bands are flat in the bulk, but close to the electrodes the valence and conduction bands in the organic layer bend due to the Ohmic nature of the contacts. Hence, in the region close to the contact, where the bands bend, a net electric field exists, which, according to Limpinsel *et al*., drives the extraction of photogenerated carriers and therefore contributes to a net voltage-independent photocurrent $J_{ph}(V_{pos})$.[6] Hence, band bending close to the electrodes would contribute to voltage-independent photocurrent that shifts the field-dependent photocurrent contribution to negative values.

Dibb *et al*. have analyzed the relationship between the linearity of the light-intensity dependence of J_{ph} and the recombination mechanism in organic solar cells.[7] They demonstrated that it is possible for a cell to exhibit a J_{ph} linear with illumination intensity even if the underlying recombination process that shapes the $J(V)$ curve is nonlinear.[7] Very recently, Petersen *et al*. studied the charge extraction and photocurrent in organic bulk heterojunction solar cells using a numerical drift-diffusion model to investigate the effects of injection barriers, selective contacts, different recombination mechanisms, and series resistance on $J_{ph}(V)$.[8] The modeling results of Petersen *et al*.[8] are qualitatively consistent with experimental observations of Ooi *et al*.[5] and Limpinsel *et al*.[6] and explain the effects by position-dependent equilibrium concentrations and lifetimes of the charge carriers.

Importantly, however, Street *et al*. showed analytically and experimentally that the series resistance in the solar cell's circuit reduces the photocurrent in forward bias.[9] This has significant implications for the interpretation of the J_{ph}-V of data presented by Ooi *et al*.[5] and Limpinsel *et al*.[6] because these authors did not correct the measured photocurrent for the series resistance of the electrodes. Consequently, the externally applied voltage deviates from the effective bias, especially in forward bias. Because the photocurrent as a function of effective voltage on the active layer is of physical relevance in understanding the field dependence of the collection of photogenerated charges, the relevance of the results described so far is ambiguous. Furthermore, in interpreting the voltage dependence of J_{ph} the possible effect of injected charge carriers has largely been neglected.[5,6] These two considerations warrant a more detailed study of photocurrents in polymer solar cells.

Therefore, in the present paper, we study experimentally and numerically the photocurrent as a function of effective voltage in polymer:fullerene bulk heterojunction devices. We name this the internal photocurrent. The experimental J_{ph}-V curves are measured with a pulsed light source setup to minimize the heating effect of the substrate. We take care to correct the experimental J_{ph}-V curve for the effect of the electrodes' series resistances and determine the internal J_{ph}-V curve as a function of the effective applied voltage V_{eff}. We study the internal photocurrent for solar cells based on poly[{2,5-bis(2-hexyldecyl)-2,3,5,6-tetrahydro-3,6-dioxopyrrolo[3,4-c]pyrrole-1,4-diyl}- *alt* -{[2,2'-(1,4-phenylene)bithiophene]-5,5'-diyl}] (PDPPTPT) with PCBM. PDPPTPT is a small band gap polymer that provides a power conversion efficiency of 4.6% in solar cells with PCBM.[10] We show that the internal photocurrent determined on PDPPTPT:PCBM devices is much larger in forward bias than the external photocurrent. For devices with low injection current, a rather symmetric J_{ph}-V curve around $J_{ph} = 0$ is observed. No voltage-independent negative photocurrent offset is observed in the internal J_{ph}-V curve for any of the devices.

We further employ numerical simulations in a drift-diffusion model,[11] similar to Petersen *et al*.,[8] to study the internal photocurrent in forward and reverse bias. In the numerical simulations, the effects of bimolecular recombination, injecting contact, and band bending on the J_{ph}-V curve are considered. The simulations show that the J_{ph}-V curves are strongly dependent on the bimolecular recombination rate. In forward bias, the photocurrent is reduced for Langevin-type recombination. When the recombination rate is increased (reduced), the photocurrent reduces (increases) in forward bias. This reduction of the photocurrent in forward bias can be related to an increased recombination between photogenerated carries and injected carriers. The simulations show that neither self-selective nor band bending is needed to observe J_{ph}-V curves, which are asymmetric around $J_{ph} = 0$.

Furthermore, simulations show an enhanced injection current under illumination for very low recombination rates or for low recombination rates and unbalanced electron and hole mobilities. This enhanced injection current under illumination is related to a modification of the net space charge and of the injection properties of the contacts under illumination. Experimentally, we observed enhanced photocurrent in unannealed and annealed P3HT:PCBM solar cells.

II. EXPERIMENT

PDPPTPT:PCBM (1:2 by weight) devices were prepared by first spin casting a 50-nm-thick PEDOT:PSS (Clevios P, VP Al4083, Heraeus) onto precleaned glass substrate covered with patterned indium tin oxide (ITO, 14 Ω sq^{-1}), followed by spin casting a 100-nm-thick PDPPTPT:PCBM layer from chloroform containing 25mg mL^{-1} 1,8-diiodooctane.[10] As back electrodes PEDOT:PSS/Ag, Ag, and LiF/Al were used. For the PEDOT:PSS/Ag device, PEDOT:PSS (Clevios F CPP105D, Heraeus) diluted with 30% vol/vol of isopropanol was spin coated on the PDPPTPT:PCBM layer. The PEDOT:PSS top

contact device was masked to avoid spurious photocurrent from areas outside the device area defined by the overlap of the two electrodes, caused by the high lateral conductivity of the Clevios F CPP105D PEDOT:PSS. Ag (100 nm), LiF (1 nm), and Al (100 nm) were thermally evaporated in a vacuum of 10^{-7} mbar. The active layer thicknesses of all the devices are determined with a Veeco Dektak 150 Surface Profiler and are ∼100 nm. J-V characteristics are measured with a Keithley 2400 source meter under illumination with a tungsten-halogen lamp with a Schott GG385 UV filter and a Hoya LB120 daylight filter at 100 mW cm^{-2} light intensity. To measure photocurrents and minimize the heating of the sample under illumination we use a solid-state laser (B&W Tek Inc., 532 nm, 30 mW) and a mechanical chopper (Stanford Research SR 540 chopper, $f = 175$ Hz) to produce a square wave-modulated illumination source. The device is connected in series to a 2.5 Ω probe resistor and voltage source. The probe resistor is connected in parallel to the input of a lock-in amplifier (Stanford Research Systems SR830), and the amplitude of the recorded signal is proportional to the photocurrent.

III. RESULTS AND DISCUSSION

A. Photocurrent in PDPPTPT:PCBM devices

To investigate J_{ph}-V curves experimentally and study the effect of injected carriers on the J_{ph}, PDPPTPT:PCBM blends were used as the active layer in three glass/ITO/PEDOT:PSS/PDPTPT:PCBM devices with three different top contacts: LiF/Al, Ag, and PEDOT:PSS/Ag. The J-V characteristics of these three devices, recorded under 100 mW cm^{-2} white-light illumination, are shown in Fig. 1(a). The device with the LiF/Al top contact shows the typical performance of a PDPTPT:PCBM solar cell with a short-circuit current $J_{sc} = 10.56$ mA cm^{-2}, an open-circuit voltage $V_{oc} = 0.79$ V, and a fill factor FF = 0.58, providing a power conversion efficiency of $\eta = 4.8\%$. For the Ag and PEDOT:PSS/Ag different top electrodes, the devices show lower performances due to the reduced V_{oc}'s of 0.74 and 0.27 V, respectively. The reduction of V_{oc} for the Ag and PEDOT:PSS/Ag top contact devices with respect to the solar cell is due to the different effective work functions of Ag and PEDOT:PSS. As can be seen from the J-V characteristics measured under illumination, the current quickly saturates in reverse bias at similar values, indicating identical transport and generation of free charge carriers in the bulk for the three devices in reverse bias. The slight changes in magnitudes of illumination current in reverse bias can be related to optical processes. Different top electrodes can result in different optical interference in the stack and, consequently, in a difference in absorption across the layer. The illumination current of the PEDOT:PSS/Ag device is symmetric around $J_{ph} = 0$ and saturates in reverse and forward bias at similar values.

The dark J-V curves clearly show the effect of the top electrodes on the dark currents J_{dark} [Fig. 1(b)]. For the LiF/Al top electrode the dark current is large in forward bias at +2 V bias; for the Ag electrode the dark current is about five times lower, while for the PEDOT:PSS/Ag device the injection current is strongly suppressed. The magnitude is related to the injecting properties of the top electrodes. The LiF/Al top electrode forms an Ohmic contact with the PCBM acceptor, which has a LUMO energy at −4.2 eV. Ag has a higher work function than LiF/Al and creates an electron injection barrier that reduces the dark current. PEDOT:PSS/Ag has the highest work function, and electrons cannot be injected such that the dark current is strongly suppressed. The low dark current

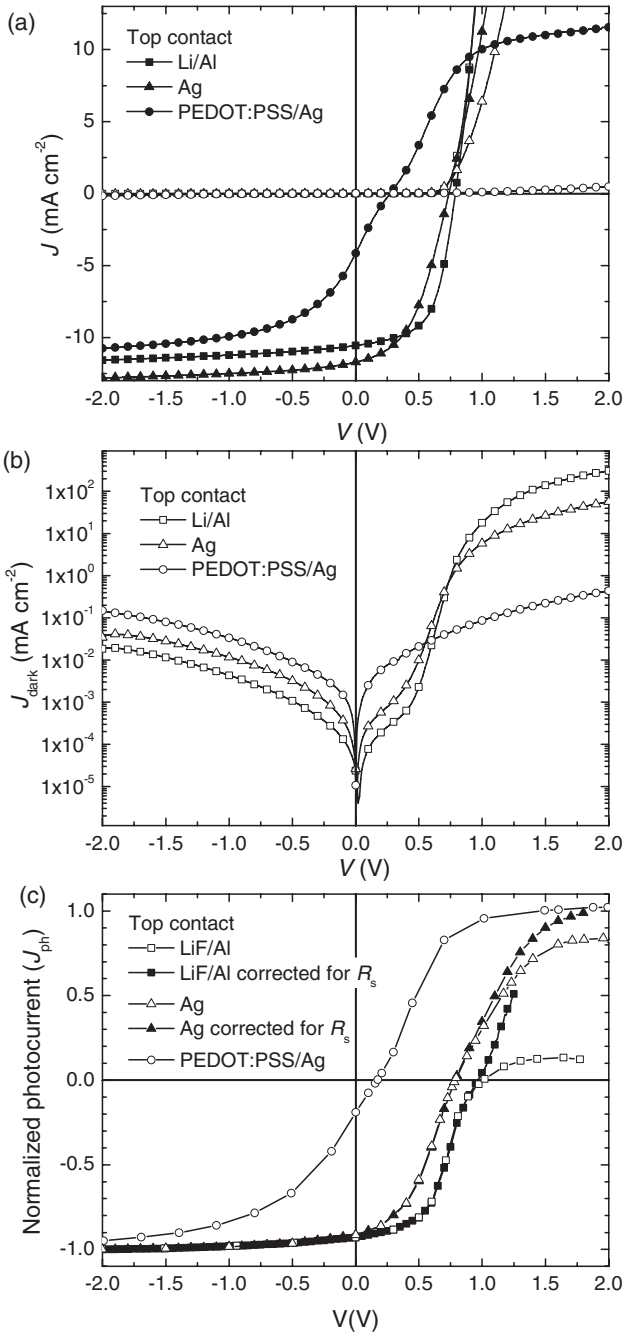

FIG. 1. J-V characteristics of ITO/PEDOT:PSS/PDPPTPT:PCBM devices with LiF/Al, Ag, and PEDOT:PSS/Ag top contacts. (a) In the dark (open symbols) and under 100 mW cm^{-2} continuous white-light illumination (solid symbols). (b) Semilogarithmic plot of the dark currents. (c) J_{ph}-V characteristics measured with modulated light before (open symbols) and after series resistance correction (solid symbols) normalized to the maximum photocurrent at reverse bias (i.e., −2 V for LiF/Al and Ag; −4 V for PEDOT:PSS/Ag).

for the ITO/PEDOT:PSS/PDPPTPT:PCBM/PEDOT:PSS/Ag device demonstrates that at both PEDOT:PSS contacts large hole and electron injection barriers are present. It also implies that for the LiF/Al and Ag devices the dark current is electron dominated. The energy difference between the HOMO of PDPPTPT (−5.5 eV)10 and the work function of PEDOT:PSS (−5.1 eV) indeed suggests a barrier of ∼0.4 eV for hole injection. From the V_{oc} (0.27 V) of the PEDOT:PSS/Ag device, we infer that at that electrode the injection barrier for holes will be larger by the same amount and is about 0.7 V. The large illumination currents in reverse and forward bias for the PEDOT:PSS/Ag device demonstrate that photogenerated carriers can be effectively collected at the PEDOT:PSS electrodes. From the efficient collection of photogenerated carriers in forward and reverse bias and from the estimated injection barriers, electrodes blocking the collection of carriers from the active layer can be excluded. The suppressed dark currents are solely due to injection barriers from the electrode to the active layer.

Since the dark current is very low in the PEDOT:PSS/Ag top contact device, the illumination current (J_{light}) is equal to the photocurrent (J_{ph}). The shape of the J_{ph}-V curve for the PEDOT:PSS/Ag top contact device corresponds to the idealized photocurrent that follows from the drift-diffusion model of Sokel and Hughes.[12] In reverse and forward bias all the photogenerated carriers are collected because the electric field is large enough and the photocurrent is only limited by the generation rate of free carriers (G).

Closer to V_{oc}, the electric field decreases, and diffusion of carriers starts to compete with the drift of carriers. Because photogenerated carriers diffuse isotropically out of the device, the diffusion current will not contribute to the net photocurrent close to V_{oc}, and the photocurrent J_{ph} is reduced. At the compensation voltage V_0 the photocurrent cancels ($J_{ph} = 0$) because the electric field in the device is minimal, and consequently, carriers either diffuse out of the device or recombine between each other.

For the LiF/Al and the Ag top contact devices the illumination current consists mainly of photocurrent below V_{oc}, and close to V_{oc} the photocurrent is low for the same reason as for the PEDOT:PSS/Ag device (diffusion and recombination). At high reverse bias the illumination current saturates since all the photogenerated carriers are collected ($J_{ph} = qGL$, with q being the elementary charge and L being the thickness). In forward bias above V_{oc} the illumination current consists of photogenerated and injected carriers. With increasing bias, the illumination current becomes quickly dominated by the injected carriers. As already mentioned by Ooi *et al.*,[5] the photocurrent cannot be reliably determined with a standard setup because the substrate and photoactive layers heat up under illumination. In such a case the photocurrent would be overestimated because under illumination and higher temperature the injected carriers have an increased mobility compared to the dark. To determine the photocurrent in forward bias accurately and minimize heating effects, we measured the PDPPTPT:PCBM devices with the pulsed setup described in Sec. II.

Figure 1(c) shows J_{ph}-V curves normalized to the maximum reverse photocurrent of the three PDPPTPT:PCBM devices measured with the pulsed light source. The photocurrent of the PEDOT:PSS/Ag device is nearly symmetric around $J_{ph} = 0$ and saturates in forward bias and reverse bias at the same maximum photocurrent that was measured with the continuous illumination setup. For the LiF/Al and Ag devices, the photocurrent is reduced in forward bias. This reduction is more pronounced for the LiF/Al electrode where the dark current is larger.

Similar to Ooi *et al.*[5] and Limpinsel *et al.*,[2] we can identify the hypothesized POS in the J_{ph}-V curves and then decompose the curves into a bias-symmetric voltage-dependent photocurrent and a constant voltage-independent photocurrent offset. An alternative view, recently proposed by Petersen *et al.*,[8] is that the photocurrent in forward bias is reduced by the injected carriers, e.g., when these recombine with photogenerated carriers. This view is supported by the correlation between a high dark current and a high reduction of J_{ph} [Figs. 1(b) and 1(c)].

However, it is important to note that for the measured J_{ph}-V curves the resistance of the electrode (mainly the ITO electrode) and the resulting voltage drop over the electrodes when current flows through the device have been neglected so far. According to Street *et al.*,[9] the series resistance of the solar-cell circuit can lead to a reduced photocurrent in forward bias. To correctly interpret the photocurrent curves it is important to determine the photocurrent versus the effective applied voltage V_{eff} on the active layer. This is justified since the transport, collection, and recombination of generated carriers is governed by the electric field across the active layer and the electric field scales with the effective (internal) voltage. To correct for the voltage drops over the electrodes and determine J_{ph} as a function of the effective voltage we first calculate the illumination current I_{light} by adding the photocurrent and the dark current ($I_{light} = I_{dark} + I_{ph}$). Then, using $V = R_s I$, the effective voltage is determined for the dark and illumination currents knowing the series resistance of the device ($R_s = 24\ \Omega$): $V_{eff} = V_{appl} - R_s I_{light/dark}$. The I-V curves in dark and under illumination versus effective voltage are then given by

$$\begin{aligned} I_{dark}(V_{eff}) &= I_{dark}[V_{appl} - I_{dark}(V_{appl})R_s], \\ I_{light}(V_{eff}) &= I_{light}[V_{appl} - I_{light}(V_{appl})R_s]. \end{aligned} \tag{1}$$

The photocurrent density is then calculated by

$$J_{ph}(V_{eff}) = [I_{light}(V_{eff}) - I_{dark}(V_{eff})]/A, \tag{2}$$

with A being the area of the illumination spot. The corrected J_{ph}-V curves are shown in Fig. 1(c) for the LiF/Al and Ag devices. For the PEDOT:PSS/Ag device, no correction is needed since the dark current is very low and the J_{ph}-V curve does not change after corrections. The corrected J_{ph}-V curve and the measured J_{ph}-V curve superimpose in the voltage range from −2 V to V_{oc} for the LiF/Al and Ag devices. In the voltage range above V_{oc} the corrected J_{ph} is somewhat larger than the noncorrected J_{ph} for the Ag device and significantly larger for the LiF/Al device.

The increase of the corrected photocurrent with respect to the noncorrected photocurrent in forward bias [Fig. 1(c)] is due to the difference in voltage drop in the dark and under illumination over the electrodes. Under illumination, the current is larger at the same applied voltage than in the dark and

therefore causes a larger voltage drop over the electrodes than in the dark. Consequently, the external illumination current measured at the same applied voltage as the dark current has a lower effective (internal) voltage V_{eff} than the dark current. This will yield a larger reconstructed internal photocurrent.

After correction the J_{ph}-V curve of the Ag top contact device is symmetric around $V_{\text{eff}} = 0.75$ V and seems to saturate in forward bias. We cannot fully exclude an increase of the photocurrent beyond the saturation current above $V_{\text{eff}} = 1.8$ V because it was difficult to measure the Ag top contact device in a larger effective voltage range because at higher current the device degrades due to switching effects.

For the LiF/Al top contact device, the internal photocurrent is much larger than the externally measured photocurrent. At $V_{\text{eff}} = 1.25$ V, J_{ph} has reached half of the reverse saturation current. Because the LiF/Al device does not remain stable at high current densities, it was not possible to measure the internal J_{ph} beyond $V_{\text{eff}} = 1.25$ V. Hence, it was not possible to determine where the photocurrent saturates. From the shape of the corrected J_{ph}-V curve of the LiF/Al device, three scenarios are possible: (i) the photocurrent saturates at maximum photocurrent and is symmetric around the compensation voltage V_0 (close to V_{oc}), similar to the PEDOT:PSS/Ag and Ag devices; (ii) the photocurrent saturates in forward bias, with J_{ph} reaching a value of 0.5–1 times the saturation current in reverse; or (iii) the photocurrent does not saturate and is larger in forward bias than the reverse bias due to a photomultiplication effect.

From these results it is clear that the strong reduction of the forward photocurrent and the significant offset of the field-dependent photocurrent due to a constant photocurrent contribution as described by Ooi *et al.*[5] and Limpinsel *et al.*[6] are not observed for any of the PDPPTPT:PCBM devices, after correcting for the effect of the series resistance R_{s}. Furthermore, because the magnitude of the dark current of the PDPPTPT:PCBM LiF/Al device is typical for polymer:fullerene solar cells and since the internal photocurrent in forward bias strongly increases with respect to the external photocurrent after correction for the series resistance, it is essential to include this correction when measuring photocurrents in organic solar cell above the V_{oc}.

In conclusion, after making appropriate corrections, we do not observe a strong influence of injected carriers on the J_{ph}-V curves of PDPPTPT:PCBM devices. We also did not observe a POS below $J_{\text{ph}} = 0$. The measurements indicate rather symmetric J_{ph}-V curves around V_0. To better understand how the J_{ph}-V curves can be affected by the injected charges, we perform numerical simulations, which are shown in Sec. III B.

B. Photocurrent simulations

To study the internal photocurrent and investigate how the shape of the internal photocurrent J_{ph}-V curve is affected by bimolecular recombination, injecting electrodes, and band bending, we use numerical drift diffusion simulation. The numerical method is described in detail elsewhere.[11] The numerical program considers diffusion and drift of free carriers in one dimension. Also, space-charge effects are included. The active layer of the solar cell is considered under the effective medium approach, meaning that electrons and holes

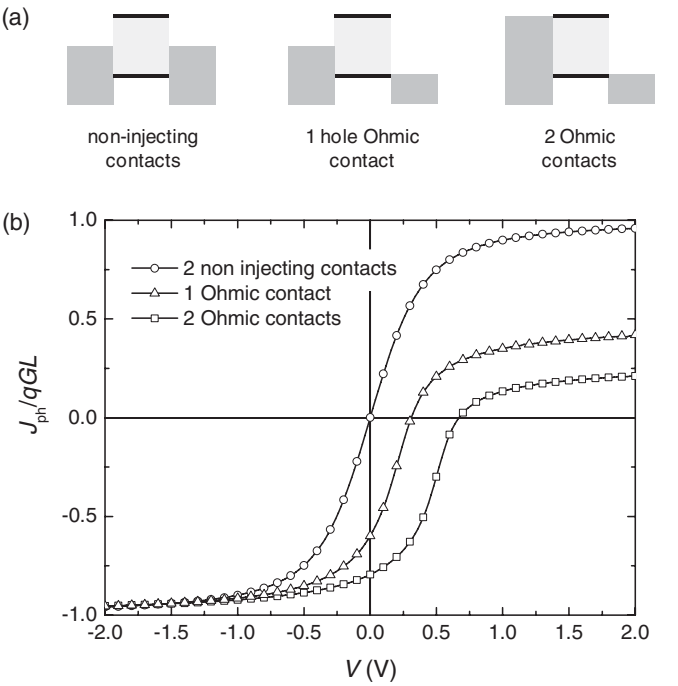

FIG. 2. (a) Schematic band diagram of the simulated devices: noninjecting contacts, a device with one Ohmic contact for holes, and a device with Ohmic electron and hole contacts. Effective band gap is $E_{\text{g}} = 1$ eV; injection barriers are either 0 or 0.5 eV. (b) Simulated J_{ph}-V characteristics normalized to the maximum photocurrent qGL of the three devices shown in (a). Layer thickness $L = 100$ nm, equal hole and $\mu_{\text{n}} = \mu_{\text{p}} = 10^{-8}$ m^2 V^{-1} s^{-1}, effective band gap $E_{\text{g}} = 1$ eV, $G = 2.7 \times 10^{27}$ m^{-3} s^{-1}, and Langevin prefactor $\gamma_{\text{pre}} = 1$ are used in the simulations.

are transported in the same phase. For sake of simplicity, we do not investigate the influence of disorder and field-dependent geminate recombination. Therefore, we use in the simulations constant carrier mobilities independent of electric field and carrier density, and the generation rate G of free carriers under illumination is considered constant, independent of the electric field and position in the device.

In the simulations a layer thickness of 100 nm is assumed. The relevant energy difference between the HOMO level of the donor and of the LUMO level of the acceptor is the effective band gap, assumed to be $E_{\text{g}} = 1$ eV in the simulations. In the simulations we consider electrodes without and with (0.5 eV) barriers for carrier injection from the electrodes [Fig. 2(a)]. Specifically, we consider three different configurations (two noninjecting contacts, two Ohmic contacts, and one noninjecting and one Ohmic contact).

Recombination between free carriers is considered by a Langevin-type recombination rate equation:[13]

$$R = \gamma_{\text{pre}} \frac{q(\mu_{\text{n}} + \mu_{\text{p}})}{\varepsilon_0 \varepsilon_{\text{r}}} \left(np - n_{\text{i}}^2\right), \tag{3}$$

where γ_{pre} is a Langevin prefactor, q is elementary charge, μ_{n} and μ_{p} are the electron and hole mobility, ε_0 is the dielectric permittivity of vacuum, ε_{r} is the relative permittivity, n and p are the electron and hole density, and n_{i} is the intrinsic carrier density. The photocurrent density J_{ph} is obtained by taking the difference between the simulated J-V curve in

the dark and under illumination. The calculated J_{ph}-V curves are normalized by the maximum photocurrent given by the generation rate of charge carriers qGL.

First, we describe the effect of different injecting contacts and bimolecular Langevin recombination ($\gamma_{pre} = 1$), following an approach similar to Petersen *et al.*[8] Complementary to Petersen *et al.* we then focus on the influence of extremely low recombination rates and of low recombination rates together with unbalanced electron-hole mobilities. Three device configurations are compared: (i) with two noninjecting contacts, (ii) with one Ohmic hole-injecting contact, and (iii) with Ohmic electron and hole-injecting contact [Fig. 2(a)]. The simulated J_{ph}-V curves for these devices for $\gamma_{pre} = 1$, $\mu_n = \mu_p = 10^{-8}$ m^2 V^{-1} s^{-1}, $E_g = 1$ eV, $G = 2.7 \times 10^{27}$ m^{-3} s^{-1} are shown in Fig. 2(b).

For the device with noninjecting contacts a symmetric J_{ph}-V curve around $V = 0$ V is obtained which saturates in forward and reverse bias.[12] The symmetric J_{ph}-V curve is expected because of the symmetric contacts, and a similar result has recently been described in Ref. 8. The exact shape of the J_{ph}-V curve will depend on the transport, extraction, and bimolecular recombination of photogenerated carriers. [12] At high reverse or forward bias, all the photogenerated carriers are collected by the electrodes, and the photocurrent is limited only by the generation rate and reaches the maximum photocurrent qGL. When the voltage is decreased from negative or positive bias to 0 V, the photocurrent decreases in magnitude. This is related to a decrease of the electric field across the device, which reduces field-assisted collection of carriers (drift), and to diffusion starting to compete with drift. At 0 V, the photocurrent is canceled because electric field is extremely low and generated carriers either diffuse isotropically out of the device or recombine bimolecularly.

When one injecting hole contact is introduced, the J_{ph}-V curves shift to the right and J_{ph} cancels at 0.31 V. This is because the built-in voltage increases when the work functions of the electrodes are different. In forward bias above 0.31 V, the photocurrent is strongly reduced with respect to the generation rate qGL and saturates at 2 V around $0.4qGL$. When two Ohmic contacts are used, the J_{ph} cancels at 0.65 V, and in forward bias J_{ph} is further reduced with respect to qGL, saturating at about $0.2qGL$.

The dark current in the simulations of the device with two injecting Ohmic contacts is larger than the dark current of the device with only one hole-injecting contact (not shown here). This is because the device becomes bipolar, and the presence of both injected electrons and holes reduces the net space at the injection contact. Consequently, more electrons and holes can be injected into the device.[14,15] The higher concentration of injected charge carriers apparently reduces the photocurrent due to bimolecular recombination with photogenerated carriers (also see Ref. 8). Note that R scales with np [Eq. (3)].

For devices with Ohmic contacts, we observe an asymmetric J_{ph}-V curve in which one can identify a POS at negative J_{ph}. In calculating this curve, Ohmic contacts have been used, and consequently, self-selective contacts are not needed to observe a POS as proposed by Ooi *et al.*[5] This conclusion was also obtained by Petersen *et al.*[8] Comparing the simulated photocurrent curves [Fig. 2(b)] for devices with injecting contacts with the experimental J_{ph}-V curves of the PDPPTPT:PCBM devices with Ag and LiF/Al top contacts [Fig. 1(c)], the photocurrent in the experiment is much larger in forward bias compared with the simulated curves. This could be related to a reduced recombination rate in the PDPPTPT:PCBM blend.

To further investigate the influence of the bimolecular recombination rate on the photocurrent, we perform simulations on the device with two Ohmic contacts and vary the recombination rate via the Langevin prefactor. Figure 3(a) depicts the normalized J_{ph}-V curves for different Langevin prefactors γ_{pre}. In reverse bias below V_0, the photocurrent decreases with increasing γ_{pre}. This is related to bimolecular recombination between photogenerated carriers (no carriers are injected in reverse bias). Increasing the recombination rate by increasing γ_{pre} decreases the fill factor [Fig. 3(a), below V_0]. In forward bias above V_0, the trend of the reduction of the photocurrent with Langevin prefactor is more pronounced. At $\gamma_{pre} = 10$ the photocurrent almost cancels, but when γ_{pre} decreases, the photocurrent increases in forward bias and the J_{ph}-V curve becomes more symmetric. The effect of lowering

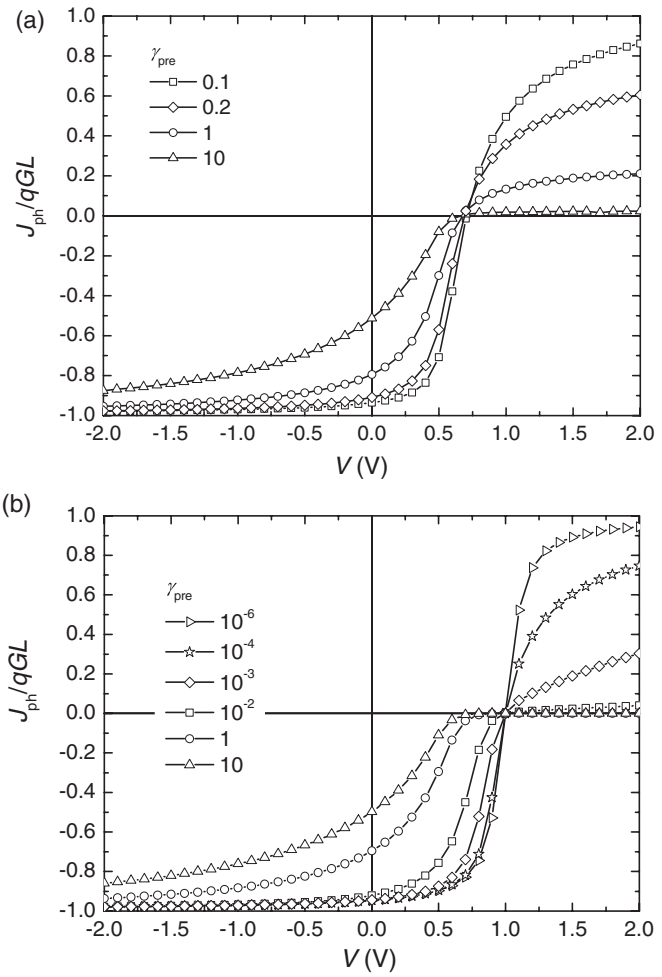

FIG. 3. (a) Simulated J_{ph}-V curves normalized to the maximum photocurrent qGL for various Langevin prefactors γ_{pre}. $L = 100$ nm, $\mu_n = \mu_p = 10^{-8}$ m^2 V^{-1} s^{-1}, $E_g = 1$ eV, $G = 2.7 \times 10^{27}$ m^{-3} s^{-1}, and two Ohmic contacts were used in the simulations. (b) Same as (a), but without band bending.

the bimolecular recombination by setting $\gamma_{pre} < 0.1$ will be discussed in Sec. III D.

The stronger response of the photocurrent to the Langevin prefactor γ_{pre} in forward bias clearly evidences that the photocurrent is reduced by bimolecular reduction between photogenerated carriers and injected carriers. In forward bias, the carrier density in the dark and under illumination is a few orders of magnitudes larger than in reverse bias due to injection of carriers. Hence, many photogenerated carriers will recombine with injected carriers, and the recombination rate (of photogenerated carriers) is limited by the injected carriers. Consequently, a modification of the recombination rate via the Langevin prefactor has a strong effect in forward bias. In reverse bias, photogenerated carriers only recombine among each other, and the recombination rate is lower because it is limited by the density of photogenerated carriers, and the effect of a change in γ_{pre} is smaller.

Limpinsel *et al.*[6] proposed that band banding has a strong influence on the J_{ph}-V curve and is the reason for the POS. Simulated J_{ph}-V curves in absence of band bending [obtained by keeping $\varphi(x) = xV/L$ via switching off the routine that solves the Poisson equation, $\nabla^2\varphi(x) = q[n(x) - p(x)]/\varepsilon_0\varepsilon_r$, in the simulations] are shown in Fig. 3(b). Comparison with Fig. 3(a) shows that the photocurrent is much more reduced in forward bias for a given γ_{pre} when there is no band bending [Fig. 3(b)] than with band bending [Fig. 3(a)]. Clearly, Figs. 3(a) and 3(b) show that the photocurrent curves are reduced due to bimolecular recombination and band bending is not needed to explain this reduction. We note that band bending is necessary to explain that the voltage at the POS is smaller than the built-in potential [compare Figs. 3(a) and 3(b)], as discussed in detail by Petersen *et al.*[8]

Summarizing, the photocurrent simulations show that the bimolecular recombination of photogenerated charge carriers with injected charge carriers can cause a significant decrease of the photocurrent in forward bias. The same conclusion was recently obtained by Petersen *et al.*[8] The decrease is strongly modulated by the extent to which bimolecular recombination occurs. In the simulations we assumed Langevin recombination of electrons and holes and adjusted the rate, using a variable prefactor γ_{pre} [Eq. (3)]. The simulations clearly show that to explain a reduction in forward bias it is not necessary to assume charge-selective contacts as suggested by Ooi *et al.*[5] Likewise, the explanation offered by Limpinsel *et al.*[6] that the reduction of the forward photocurrent is due to band-bending effects near the electrode does not seem correct because under conditions where band bending was excluded, the reduction of photocurrent in forward bias is even higher than when incorporating band bending.

C. Forward photocurrent model

The effects of reduced photocurrent under forward bias as a result of recombination with injected charge carriers that emerge from the simulations (Fig. 3) can be rationalized with a simple analytical model. For that we first consider the situation of a device with a single Ohmic contact that injects holes under forward bias and assume that the charge-carrier mobilities for electrons and holes are equal ($\mu = \mu_n = \mu_p$). Under continuous illumination the rate equation for photogenerated electrons n_{ph} reaches steady state, i.e.,

$$\frac{dn_{ph}}{dt} = G - R - \frac{n_{ph}}{\tau} = 0, \tag{4}$$

with τ being the lifetime of the photogenerated electrons. In high forward bias the density of injected holes p_{inj} will largely exceed the density of photogenerated holes p_{ph}, such that the Langevin recombination rate can be expressed as

$$R = \gamma_{pre}\frac{q\mu}{\varepsilon_0\varepsilon_r}n_{ph}p_{inj}. \tag{5}$$

In high forward bias we further consider that drift dominates diffusion of charges such that the lifetime of the photogenerated electrons is determined by their average drift time τ_{drift}. Neglecting space-charge effects, the electric field equals V/L, and since, on average, photogenerated electrons need to traverse only half of the active layer in order to reach an electrode, the lifetime is given by[16]

$$\frac{1}{\tau} = \frac{1}{\tau_{drift}} = 2\frac{\mu V}{L^2}, \tag{6}$$

such that the photocurrent density, which is the extraction rate of photogenerated charges, equals

$$J_{ph} = \frac{qn_{ph}L}{\tau_{drift}}. \tag{7}$$

To determine the density of injected holes p_{inj} in high forward bias, we consider the injected current to be space charge limited, such that the average density of injected holes can be expressed as[17]

$$\bar{p}_{inj} = \frac{3}{2}\frac{\varepsilon_0\varepsilon_r}{q}\frac{V}{L^2}. \tag{8}$$

Combining (4)–(8) results in a remarkably simple expression for the photocurrent under high forward bias:

$$J_{ph} = \frac{qGL}{1 + \frac{3}{2}\gamma_{pre}}. \tag{9}$$

Figure 4(a) shows the simulated photocurrent for the device under consideration, i.e., having one injecting contact. For a device with unmodified Langevin recombination ($\gamma_{pre} = 1$), J_{ph}/qGL equals 0.46 at $V = +5$ V, close to the value of 0.40 expected from Eq. (9). Also for other values of γ_{pre} Eq. (9) yields results that are in good agreement with those obtained in the simulations [Fig. 4(b)].

For a device that has two injecting contacts instead of one, i.e., injection of both electrons and holes, the situation changes. As a result of space-charge neutralization, more carriers will be injected than expected on the basis of Eq. (8).[15] This increased carrier concentration leads to an enhanced Langevin recombination rate, which reduces J_{ph}. By including an adjustable prefactor ξ to account for this effect, the photocurrent under high forward bias can be expressed as

$$J_{ph} = \frac{qGL}{1 + \xi\gamma_{pre}}. \tag{10}$$

Figure 4(c) shows the simulated J_{ph}/qGL at $V = +2$ V for a device with electron- and hole-injecting contacts and the result of Eq. (10) for $\xi = 4$. Given the crudeness of the approach, the correspondence is rather good and shows that the analysis captures the essential physics correctly.

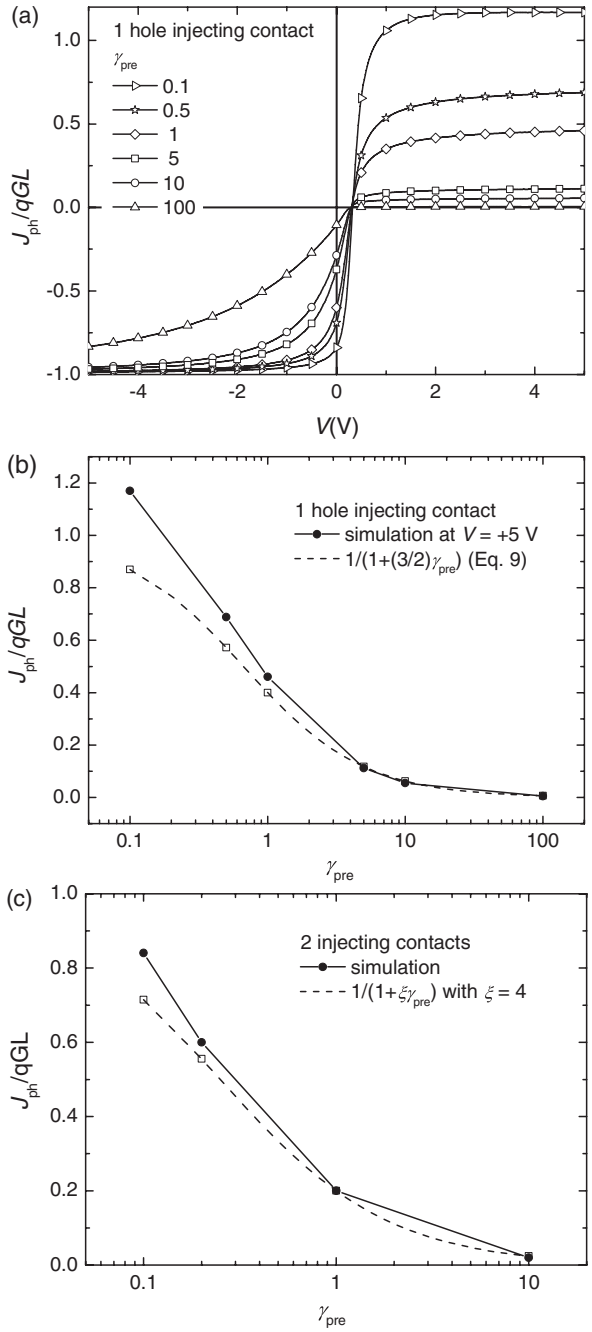

FIG. 4. (a) Simulated J_{ph}-V characteristics normalized to the maximum photocurrent qGL of a device with one hole-injecting contact, $L = 100$ nm, $\mu_n = \mu_p = 10^{-8}$ m^2 V^{-1} s^{-1}, $E_g = 1$ eV, and $G = 2.7 \times 10^{27}$ m^{-3} s^{-1} for different Langevin prefactors γ_{pre}. (b) Comparison of J_{ph}/qGL at +5 V as obtained from the simulations as shown in (a) and the value predicted from. Eq. (9). (c) Comparison of J_{ph}/qGL at +5 V obtained from the simulations for two injecting contacts and the value predicted from Eq. (10) using $\xi = 4$.

D. Photocurrent multiplication

In Secs. III B and III C, we have shown that Langevin recombination with injected charge carriers can result in a reduction of the forward photocurrent. The extent of Langevin recombination, parameterized via γ_{pre}, determines the reduction of J_{ph} in forward bias via Eq. (10). When γ_{pre} is

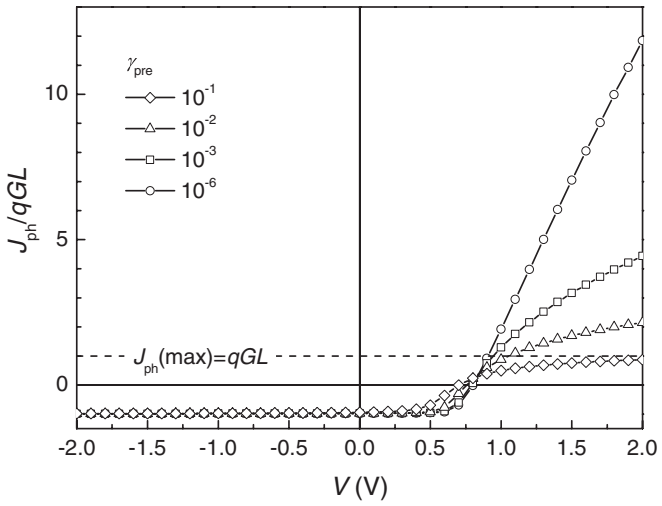

FIG. 5. J_{ph}-V curves normalized to the maximum photocurrent qGL for different low Langevin prefactors (γ_{pre}). $L = 100$ nm, $\mu_n = \mu_p = 10^{-8}$ m^2 V^{-1} s^{-1}, $E_g = 1$ eV, $G = 2.7 \times 10^{27}$ m^{-3} s^{-1}. Two Ohmic contacts were used in the simulations, and band bending is considered.

significantly reduced, an interesting observation can be made, as seen in Fig. 5, where the J_{ph}-V curves are shown for a device with two injecting contacts when band bending is taken into account. For $\gamma_{pre} < 0.1$ the photocurrent becomes much larger in forward bias than the maximum current expected from the generation rate qGL. This is striking since the current due to photogenerated charges is principally limited by the generation rate. Moreover Eqs. (9) and (10) do not predict this behavior. The fact that in the calculated J_{ph}-V characteristics with $\gamma_{pre} < 0.1$ the photocurrent is much larger than qGL can only be explained by a larger injection under illumination than in the dark. Conceptually, the calculated photocurrent can be expressed as

$$J_{ph}^{calc} = J_{light}^{photogenrated} + J_{light}^{injected} - J_{dark}^{injected} \quad (11)$$

If $J_{light}^{injected} > J_{dark}^{injected}$, the photocurrent exceeds $J_{light}^{photogenerated}$ and hence qGL. Such a photoenhanced injection was observed in some organic devices[18–21] and is known as photomultiplication.

To better understand what causes photomultiplication and illumination-enhanced injection we look at the carrier-density profile across the layer. Figure 6(a) shows the difference in electron density in the device under illumination and in the dark, $\Delta n(x) = n_{light}(x) - n_{dark}(x)$, as a function of position x in the device for $\gamma_{pre} = 10^{-1}$ and $\gamma_{pre} = 10^{-3}$ at an applied voltage of 1.5 V. The Δn can be considered as the additional electron density that is created under illumination. The additional hole density under illumination $\Delta p(x) = p_{light}(x) - p_{dark}(x)$ versus x is the mirror symmetric to $\Delta n(x)$ at $x = 50$ nm because equal hole and electron mobilities and two Ohmic contacts are used.

Figure 6(a) shows that upon reducing the γ_{pre} from 10^{-1} to 10^{-3} $\Delta n(x)$ increases because of the reduced recombination of photogenerated electrons with holes. Close to the hole-injecting contact a bump is observed at $x = 92$ nm for $\gamma_{pre} = 10^{-1}$ and at $x = 97$ nm for $\gamma_{pre} = 10^{-3}$ in the profile of $\Delta n(x)$. Beyond this bump $\Delta n(x)$ decreases

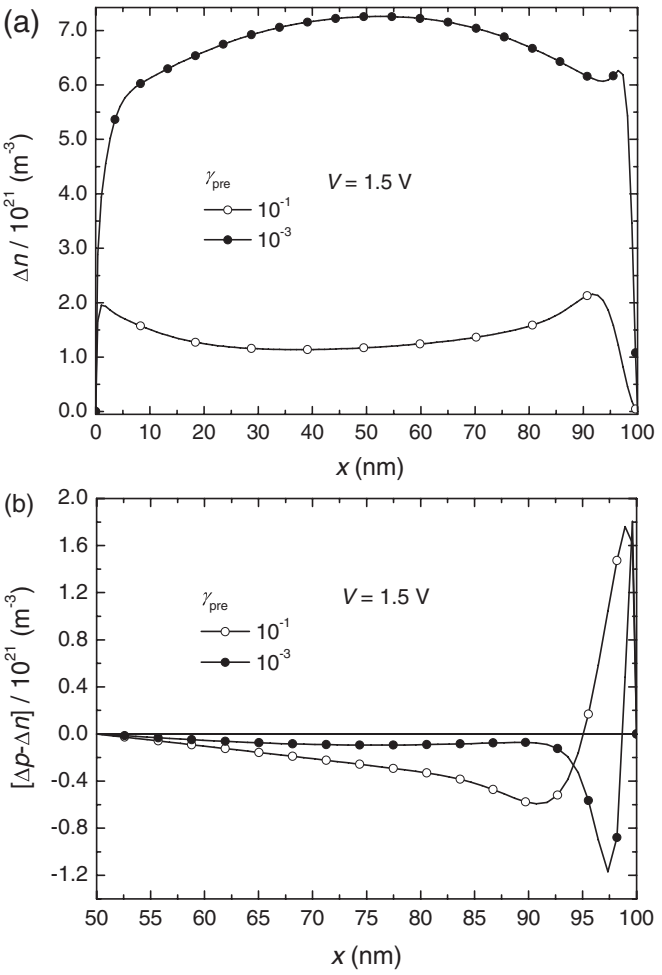

FIG. 6. (a) Additional electron density $\Delta n(x) = n_{\text{light}}(x) - n_{\text{dark}}(x)$ under illumination for Langevin prefactors $\gamma_{\text{pre}} = 10^{-1}$ and 10^{-3}. (b) Difference between the additional hole density $\Delta p(x)$ and electron $\Delta n(x)$ densities across the solar cell under illumination for Langevin prefactors 10^{-1} and 10^{-3}. $L = 100$ nm, $\mu_n = \mu_p = 10^{-8}$ m^2 V^{-1} s^{-1}, $E_g = 1$ eV, $G = 2.7 \times 10^{27}$ m^{-3} s^{-1}. Two Ohmic contacts were used in the simulations. The electron injecting contact is at $x = 0$ nm, and the hole-injecting contact is at $x = 100$ nm.

abruptly, which is due to a significant increase of bimolecular recombination between electrons and holes because the hole concentration increases several orders of magnitudes close to the hole-injecting contact. Accumulation of photogenerated electrons (holes) close to the hole (electron) injecting contact modifies the space charge at the contact and promotes hole (electron) injection, leading to an enhanced injection under illumination.[14]

To verify how the space charge is modified under illumination we plot in Fig. 6(b) $\Delta p(x) - \Delta n(x)$, which is the difference between the additional hole and electron densities and corresponds to the net space-charge change under illumination. If $\Delta p - \Delta n = 0$, the net space is not modified under illumination, but for $\Delta p - \Delta n \neq 0$ the net space charge has changed by the illumination. Figure 6(b) shows the $\Delta p - \Delta n$ profile for $\gamma_{\text{pre}} = 10^{-1}$ and $\gamma_{\text{pre}} = 10^{-3}$ at a voltage of 1.5 V. Clearly, the net space charge is modified under illumination. The most noticeable changes in net space charge (Δp–Δn) occur in the region $x = 85$–100 nm, i.e., close to the hole-injecting contact. For $\gamma_{\text{pre}} = 10^{-1}$ a negative peak in Δp–Δn is observed at $x = 91$ nm, and Δp–Δn changes sign at $x = 95$ nm. Decreasing γ_{pre} to 10^{-3}, the negative peak in Δp–Δn shifts to $x = 97$ nm and increases in magnitude; Δp–Δn changes sign around $x = 98$ nm. The shift of the negative peak of Δp–Δn (i.e., an enhanced electron density) closer to the hole-injecting contact when γ_{pre} is decreased from 10^{-1} to 10^{-3} will enhance hole injection under illumination. Likewise, electron injection is enhanced at the electron-injecting contact under illumination because the device is symmetric. The enhanced injection for a decreasing bimolecular recombination rate for $\gamma_{\text{pre}} < 10^{-1}$ results from a modification of the net space charge under illumination by the photogenerated carriers. This effect is the most pronounced for very low Langevin prefactors from $\gamma_{\text{pre}} = 10^{-3}$–$10^{-6}$. We note that for P3HT:PCBM solar cells, Langevin prefactors in the range $10^{-4} < \gamma_{\text{pre}} < 1$ have been reported in different experimental studies.[22–27]

The simulations have shown that bimolecular recombination processes are crucial in determining the photocurrent by causing photogenerated and injected carriers to recombine and by changing the space-charge distribution under illumination. Both the bimolecular Langevin recombination rate and the space-charge distribution are also influenced by the mobilities of the charge carriers. Until now we assumed $\mu_n = \mu_p = 10^{-8}$ m^2 V^{-1} s^{-1}. To investigate the effect of unbalanced mobilities ($\mu_n \neq \mu_p$) we simulated J_{ph}-V curves for $\gamma_{\text{pre}} = 0.1$ using a constant hole mobility $\mu_p = 10^{-8}$ m^2 V^{-1} s^{-1} but an electron mobility that changes from $\mu_n = 10^{-8}$ to 10^{-11} m^2 V^{-1} s^{-1} (Fig. 7). Figure 7(a) shows that if the electron mobility is reduced with respect to the hole mobility, the normalized photocurrent larger in forward bias becomes larger than unity. This evidences that at moderately low Langevin prefactors and unequal hole and electron mobilities photoenhanced injection occurs.

We verified that for $\gamma_{\text{pre}} = 1$ the photocurrent remains below the saturation current for highly dissimilar mobilities, although J_{ph}/qGL is higher in forward bias compared to equal mobilities. The latter result can be related to the fact that the injected carriers with the highest mobility dominate the recombination with the photogenerated carriers because the density of the injected carriers with lowest mobility will decrease quickly close to its injecting contact due to recombination with the other injected carrier.

The change of the net positive space charge under illumination with respect to the dark (Δp–Δn) is plotted in Fig. 7(b) as a function of position in the devices. A clear change and an absolute increase across the Δp–Δn profile is observed when the electron mobility is decreased from $\mu_n = 10^{-8}$ to 10^{-11} m^2 V^{-1} s^{-1}. This shows that for unequal electron and hole mobilities and $\gamma_{\text{pre}} = 0.1$, the net space charge is significantly different under illumination compared to the dark, explaining the changes in photocurrent [Fig. 7(a)].

The enhanced injection under illumination for unequal mobilities and $\gamma_{\text{pre}} = 0.1$ can, tentatively, be rationalized by considering (i) that recombination is low enough to allow accumulation of photogenerated carriers and (ii) that the slower photogenerated electron resides longer than the faster extracted photogenerated hole. Therefore photogener-

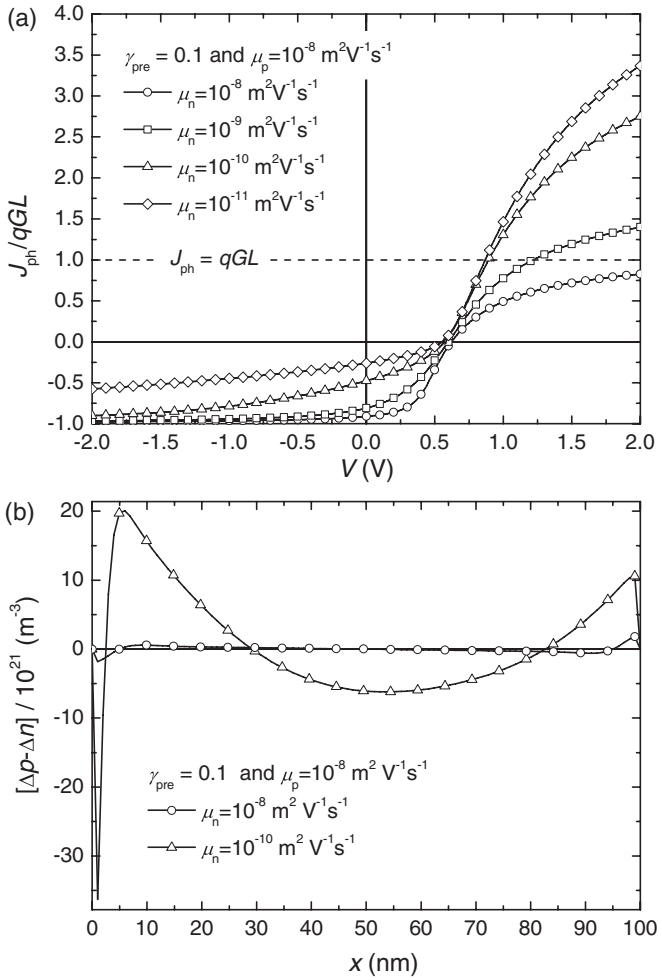

FIG. 7. (a) Simulated J_{ph}-V curves normalized to the maximum photocurrent qGL. Two Ohmic contacts were used in the simulations and $L = 100$ nm, $E_g = 1$ eV, $G = 2.7 \times 10^{27}$ m^{-3} s^{-1}, $\gamma_{pre} = 0.1$, $\mu_p = 10^{-8}$ m^2 V^{-1} s^{-1}, and $\mu_n = 10^{-8}$–10^{-11} m^2 V^{-1} s^{-1}. (b) Difference between the additional hole (Δp) and electron (Δn) densities under illumination for different $\mu_n = 10^{-8}$ and 10^{-10} m^2 V^{-1} s^{-1}.

ated electrons accumulate more than the photogenerated holes in the device, creating a charge imbalance, which has to be compensated by additional injection of holes.

In conclusion, the simulations show that photocurrent multiplication can result from a modification of the space charge under illumination either when the recombination rates are extremely low or when the recombination rate is reduced and charge transport is unbalanced.

E. Photocurrent multiplication in P3HT:PCBM devices

The experimentally measured and corrected J_{ph}-V curves of the PDPPTPT:PCBM devices provided no clear evidence for a photoenhanced injection in forward bias [Fig. 1(c)]. However, in thick ($L = 500$ nm) P3HT:PCBM solar cells the signatures of photoenhanced injection of carriers in forward bias can be observed.

Figure 8(a) shows the dark and illumination J-V characteristics measured under continuous 100 mW cm^{-2} white-light

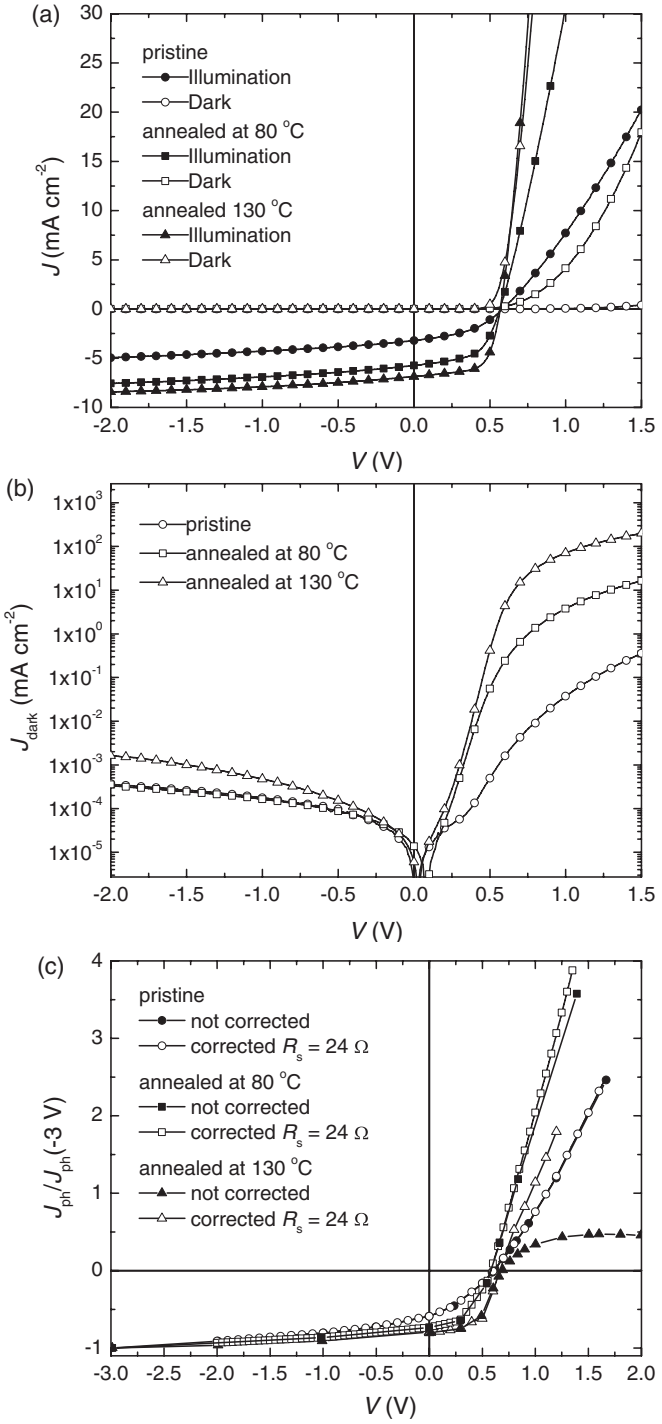

FIG. 8. (a) J-V characteristics of a 500-nm-thick P3HT:PCBM solar cell for various annealing steps. (b) Semilogarithmic plot of the dark currents. (c) J_{ph}-V curves measured with modulated light source before (solid symbols) and after (open symbols) correction for the effect of the series resistance for the same P3HT:PCBM solar cells shown in (a).

illumination of a ITO/PEDOT:PSS/P3HT:PCBM/LiF/Al solar cell before annealing (pristine) and after annealing at 80 °C for 10 min and at 130 °C for 30 min. The performance of the P3HT:PCBM solar cells increases with the annealing steps. This is well known and is related to a better crystallization of

P3HT and PCBM, improved phase separation, and enhanced charge-carrier mobilities.[28,29] The dark J-V characteristics show low leakage currents in reverse bias for all the annealing steps [Fig. 8(b)]. Without annealing the device has a very low dark current in forward bias due to the low hole mobility of the unannealed P3HT (3×10^{-12} m^2 V^{-1} s^{-1}) in the blend.[29] When the device is annealed, the dark current increases due to an improved hole mobility upon P3HT crystallization. A striking observation in Fig. 8(a) is the significant increase of the forward current upon illumination compared to the dark for the pristine device and the device annealed at 80 °C. This significant difference between the illumination current and dark current cannot be attributed to the photocurrent because it is much larger than the reverse saturation photocurrent and also not to heating of the solar cell under illumination. The large increase of the current in forward bias under illumination strongly indicates a photoenhanced injection of carriers. After the solar cell is annealed at 130 °C no significant difference in the current density in the dark and under illumination can be seen in the J-V characteristics.

To exclude the heating effects and measure the photocurrent accurately, the J_{ph}-V curves were measured with pulsed illumination for the different annealing steps of the solar cell. The corresponding J_{ph}-V curves are shown in Fig. 8(c), before and after correcting for the series resistance ($R_s = 24$ Ω). The uncorrected and corrected J_{ph}-V curves before and after annealing at 80 °C superimpose in reverse bias and do not show a significant difference in forward bias because the dark currents are low for these measurements. After annealing the solar cell at 130 °C, the corrected J_{ph}-V curve shows a much larger photocurrent in forward bias than the uncorrected J_{ph}-V curve. This increase of the photocurrent after correction is due to the large injection current of the solar cell in forward bias and due to the voltage drop at electrodes after annealing at 130 °C, similar to the results obtained for the ITO/PEDOT:PSS/PDPPTPT:PCBM/LiF/Al devices [Fig. 1(c)].

For each of the three P3HT:PCBM cells, the corrected J_{ph} normalized to the reverse saturation photocurrent [Fig. 8(c)] is larger than unity in forward bias. Thus for all the annealing steps photoenhanced injection of charge carriers is observed in forward bias. Comparing the normalized photocurrent at 1.2 V for the different annealing steps, the effect of photoenhanced carrier injection is larger after annealing at 80 °C than at 130 °C and lowest before annealing. This trend can qualitatively be explained by considering simultaneously the effect of the reduced Langevin prefactor and the effect of unbalanced charge transport on the injection current under illumination, as shown in the simulations in Figs. 7(a) and 7(b), respectively. When P3HT:PCBM is annealed, the hole mobility is improved by about three orders of magnitude, while the electron mobility does not vary significantly.[29] For instance, in pristine P3HT:PCBM devices hole mobilities are $\mu_p = 10^{-12}$ m^2 V^{-1} s^{-1}, but after annealing at 130 °C the hole mobility increases to 10^{-8} m^2 V^{-1} s^{-1}. The electron mobility increases from $\mu_n = 10^{-8}$ m^2 V^{-1} s^{-1} to 10^{-7} m^2 V^{-1} s^{-1} in the same range.[29] By studying the bimolecular recombination we recently showed that the Langevin prefactor depends on and decreases with annealing temperature.[16] The estimated γ_{pre} is 0.3 after annealing at 100 °C and 0.09 after annealing at 130 °C.[16] The reduction of γ_{pre} with annealing temperature is likely due to a more extended phase separation in the P3HT:PCBM blend with annealing temperature,[28] reducing the probability of recombination.

The photoenhanced injection of charge carriers is lowest for the pristine device. For this device the electron and hole mobilities are the most unbalanced, but the Langevin prefactor is likely close to unity as a consequence of the intimate mixing, and the photoenhanced injection of carriers is small. By annealing to 130 °C, the Langevin prefactor is reduced ($\gamma_{pre} = 0.09$),[16] but the electron and hole mobilities become much more balanced. These two opposing effects cause the result that the photoenhanced injection of charge carriers and photocurrent multiplication are not strongly increased. Figure 8(c) shows that at 80 °C, the photoenhanced current is largest after annealing at 80 °C. This can attributed to a low Langevin prefactor and a more unbalanced hole and electron mobilities than after annealing at 130 °C.

IV. CONCLUSIONS

We have studied the photocurrent in polymer solar-cell devices under forward and reverse bias experimentally and by performing device simulations using a drift-diffusion model. In the literature examples of reduced photocurrents in forward bias have been reported.[5,6] We show that these observations are likely significantly and at least partly obscured by the fact that in forward bias the effective voltage over the solar cells is much less than the applied voltage because of a non-negligible series resistance in the electrodes. After correcting for this effect we were not able to find experimental confirmation for reduced photocurrents in forward bias for efficient PDPPTPT:PCBM and pristine and thermally annealed P3HT:PCBM solar cells.

Drift-diffusion simulations have been used to identify the conditions under which reduced photocurrents in forward bias may occur. In accordance with recent results by Petersen *et al.*,[8] we find that the prime cause for a reduced photocurrent in forward bias is bimolecular, Langevin-type recombination of photogenerated and injected electron and holes carriers. Under conditions where Langevin recombination is effective, the forward photocurrent is small. Neither charge-selective contacts[5] nor band bending[6] are needed to explain a reduced forward photocurrent. The latter actually works in the opposite direction because it reduces charge injection. A simple analytical model shows that under high forward bias the photocurrent J_{ph} relative to the generation rate qGL can be expressed as $J_{ph}/qGL = (1+\xi\gamma_{pre})^{-1}$, with γ_{pre} being the Langevin prefactor and ξ being a positive constant.

Under conditions where Langevin recombination is very low or when electron and hole mobilities are unbalanced combined with a reduced bimolecular recombination, it is possible that the forward photocurrent is enhanced above the generation rate of charge carriers, such that photocurrent multiplication occurs. This effect is caused by a change in the space charge in the device under illumination, such that more carriers are injected in light than in dark. As the space-charge change by illumination is largest when the bimolecular recombination rate constant is low or when mobilities are unbalanced, the parameters contribute to conditions for finding photocurrent

multiplication in polymer solar cells. Experimentally, these effects were quantitatively demonstrated in P3HT:PCBM solar cells.

Summarizing, forward photocurrents in polymer solar-cell devices are largely affected by injected charge carriers. A reduced forward photocurrent is expected when photogenerated carriers can effectively recombine with injected charges (see also Ref. 8). An enhanced forward photocurrent occurs when recombination is low and the photogenerated charges change the space charge in the cell such that more charges can be injected. When the contacts to the device are noninjecting, the photocurrent is symmetric around the compensation voltage and maximized by the generation rate.

ACKNOWLEDGMENTS

We thank Johan Bijleveld for preparing PDPPTPT. The research was supported by a TOP grant of the Chemical Sciences (CW) division of the Netherlands Organization for Scientific Research (NWO) and is part of the Joint Solar Programme (JSP). The JSP is cofinanced by the Foundation for Fundamental Research on Matter (FOM), Chemical Sciences of NWO, and the Foundation Shell Research. This work was further supported by the Deutsche Forschungsgemeinschaft under Priority Programme 1355 "Elementary Processes of Organic Photovoltaics" and by the "Europees Fonds voor Regionale Ontwikkeling" (EFRO) in the Interreg IV-A project Organext.

[1] *Organic Photovoltaics: Materials, Device Physics, and Manufacturing Technologies*, edited by C. Brabec, U. Scherf, and V. Dyakonov (Wiley-VCH, Weinheim, 2008).
[2] D. Veldman, S. C. J. Meskers, and R. A. J. Janssen, Adv. Funct. Mater. **19**, 1939 (2009).
[3] K. Vandewal, K. Tvingstedt, A. Gadisa, O. Inganäs, and J. V. Manca, Nat. Mater. **8**, 904 (2009).
[4] V. D. Mihailetchi, P. W. M. Blom, J. C. Hummelen, and M. T. Rispens, J. Appl. Phys. **94**, 6849 (2003).
[5] Z. E. Ooi, R. Jin, J. Huang, Y. F. Loo, A. Sellinger, and J. C. deMello, J. Mater. Chem. **18**, 1644 (2008).
[6] M. Limpinsel, A. Wagenpfahl, M. Mingebach, C. Deibel, and V. Dyakonov, Phys. Rev. B **81**, 085203 (2010).
[7] G. F. A. Dibb, T. Kirchartz, D. Credgington, J. R. Durrant, and J. Nelson, J. Phys. Chem. Lett. **2**, 2407 (2011).
[8] A. Petersen, T. Kirchartz, and T. A. Wagner, Phys. Rev. B **85**, 045208 (2012).
[9] R. A. Street, K. W. Song, and S. Cowan, Org. Electron. **12**, 244 (2011).
[10] J. C. Bijleveld, V. S. Gevaerts, D. Di Nuzzo, M. Turbiez, S. G. J. Mathijssen, D. M. de Leeuw, M. M. Wienk, and R. A. J. Janssen, Adv. Mater. **22**, E242 (2010).
[11] L. J. A. Koster, E. C. P. Smits, V. D. Mihailetchi, and P. W. M. Blom, Phys. Rev. B **72**, 085205 (2005).
[12] R. Sokel and R. C. Hughes, J. Appl. Phys. **53**, 7414 (1982).
[13] P. Langevin, Ann. Chim. Phys. **28**, 433 (1903).
[14] R. H. Parmenter and W. Ruppel, J. Appl. Phys. **30**, 1548 (1959).
[15] L. M. Rosenberg and M. A. Lampert, J. Appl. Phys. **41**, 508 (1970).
[16] L. J. A. Koster, M. Kemerink, M. M. Wienk, K. Maturová, and R. A. J. Janssen, Adv. Mater. **23**, 1670 (2011).
[17] M. A. Lampert and P. Mark, *Current Injection in Solids* (Academic, New York, 1970).
[18] M. Hiramoto, T. Imahigashi, and M. Yokoyama, Appl. Phys. Lett. **64**, 187 (1994).
[19] R. N. Marks, J. J. M. Halls, D. D. C. Bradley, R. H. Friend, and A. B. Holmes, J. Phys. Condens. Matter **6**, 1379 (1994).
[20] K. Nakayama, M. Hiramoto, and M. Yokoyama, Appl. Phys. Lett. **76**, 1194 (2000).
[21] J. R. Reynaert, V. I. Arhipov, P. Heremans, and J. Poortmans, Adv. Funct. Mater. **16**, 784 (2006).
[22] A. Pivrikas, G. Juška, A. J. Mozer, M. Scharber, K. Arlauskas, N. S. Sariciftci, H. Stubb, and R. Österbacka, Phys. Rev. Lett. **94**, 176806 (2005).
[23] G. Sliaužys, G. Juška, K. Arlauskas, A. Pivrikas, R. Österbacka, M. Scharber, A. Mozer, and N. S. Sariciftci, Thin Solid Films **511–512**, 224 (2006).
[24] G. Juška, G. Sliaužys, K. Genevičius, K. Arlauskas, A. Pivrikas, M. Scharber, G. Dennler, N. S. Sariciftci, and R. Österbacka, Phys. Rev. B **74**, 115314 (2006).
[25] C. G. Shuttle, B. O'Regan, A. M. Ballantyne, J. Nelson, D. D. C. Bradley, and J. R. Durrant, Phys. Rev. B **78**, 113201 (2008).
[26] C. Deibel, A. Baumann, A. Wagenpfahl, and V. Dyakonov, Synth. Met. **159**, 2345 (2009).
[27] G. Juška, K. Genevičius, N. Nekrašas, G. Sliaužys, and R. Österbacka, Appl. Phys. Lett. **95**, 013303 (2009).
[28] X. Yang, S. C. Veenstra, W. J. H. Verhees, M. M. Wienk, R. A. J. Janssen, J. M. Kroon, M. A. J. Michels, and J. Loos, Nano Lett. **5**, 579 (2005).
[29] V. D. Mihailetchi, H. X. Xie, B. de Boer, L. J. A. Koster, and P. W. M. Blom, Adv. Funct. Mater. **16**, 699 (2006).